WAVENUMBER-DOMAIN METHOD FOR SOURCE RECONSTRUCTION FROM FAR-FIELD ARRAY MEASUREMENTS IN FLOW

Fabio Casagrande Hirono, Phillip Joseph, Filippo Maria Fazi
Institute of Sound and Vibration Research, University of Southampton, UK
University Road, Southampton, UK, SO17 1BJ.

Abstract

This paper covers the relationship between the far-field sound radiation of a planar acoustic source in the presence of a mean flow and the Spatial Fourier Transform of the source strength distribution, and proposes an inverse approach for source strength estimation from far-field data. It is shown that each microphone effectively "samples" the source wavenumber spectrum at a specific wavenumber associated to its position; hence, a particular microphone array geometry and location is inherently linked to a "visibility region" in the source wavenumber domain, and the array performance is directly related to which wavenumber spectrum components it is able to observe. It is also shown that this method is analytically equivalent to a classical frequency-domain beamforming when assuming far-field-approximated transfer functions.

1 INTRODUCTION

While much research is done in acoustics in order to understand noise generation mechanisms, some sources are hardly observable through direct measurements. In such cases, one can alternatively estimate the strength of an acoustic source from measurements of its radiated field. However, such procedure also pose its own set of challenges; for distributed sources, such as vibrating plates, estimating the source strength distribution is further complicated by interference between coherent source regions, particularly when measurements are performed close to the source.

One form to tackle this difficulty is by considering the acoustic field far from the source, away from zones of strong mutual interference. In the so-called *far-field*, the acoustic pressure can be determined from the Spatial Fourier Transform - evaluated in the wavenumber domain - of the

source strength distribution; hence, we can consider applying an Inverse Fourier Transform-type approach to estimate the source distribution from the far-field sound measurements.

This paper presents a framework encompassing far-field sound radiation and source estimation in a moving medium using the Spatial Fourier Transform; this framework naturally encompasses sound propagation in a steady medium, and can be easily extended to consider cross-spectral information when dealing with random sources. The present method also provides alternative explanations of some known limitations of classical array signal processing: for example, the effects of a finite array angular aperture and array positioning with respect to the source; the effects of the inherent sampling of the acoustic field by discrete microphones; and the effects of convection on the source estimation process.

The proposed setup is shown in Figure 1. We consider a rectangular planar radiator immersed in a moving medium with Mach number $M_x = U_x/c_0$ in the $+x$ direction; the radiator is modelled as a planar distribution of point monopole sources. The microphone array is located over a hemisphere around the source at a distance R, and we assume the microphones are in the acoustic *far-field* of the planar radiator.
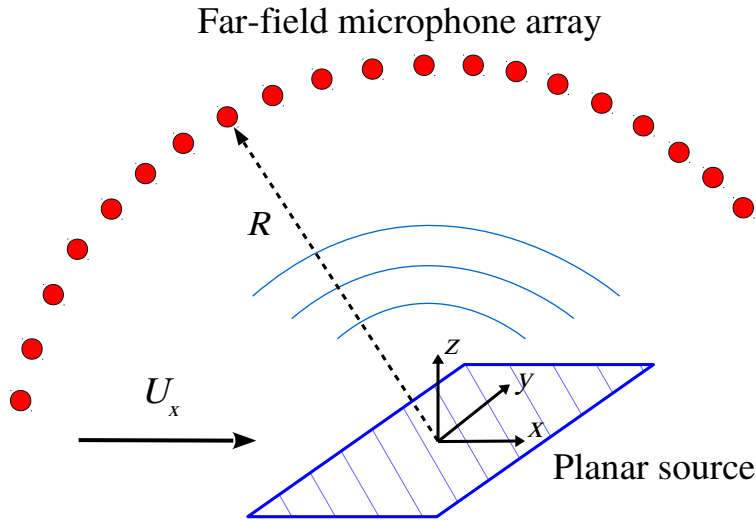

Figure 1: Experimental setup diagram.

The remainder of the paper is as follows: Section 2 discusses in more details what is meant by assuming far-field conditions and when such assumption can be considered valid, and Section 3 presents the Spatial Fourier Transform. Section 4 describes the radiation of planar sources in flow in the near-field, and shows how the acoustic far-field is analogous to a Spatial Fourier Transform; it then presents the Inverse Fourier Transform method for source estimation from far-field measurements, and briefly discusses some of the characteristics of the proposed method. Section 5 describes the problem in matrix form and compares its formulation to classical frequency-domain beamforming. Section 6 presents some simulated test cases with a single-frequency planar radiator, where different far-field array geometries are considered and their performance compared. Finally, Section 7 presents the conclusions.

2 THE FAR-FIELD APPROXIMATION

Closed-form analytical expressions for the acoustic radiation of a known sound source are generally not available for any observer location; however, simplified closed-form expressions can be obtained with the (geometrical) far-field approximation, or *Fraunhofer* approximation. This form of approximation is widely known and has been described in various textbooks [5, 8, 12]. However, not many authors in the acoustics community refer to it as the *Fraunhofer Approximation*, as it is known in the optics community for describing diffraction[9]; consequently, the same method is often presented in slightly different forms, with little effort being made in highlighting its similarities or limitations.

Let us assume a planar acoustic source, such as a vibrating plate, with $\mathbf{x}_s = (x_s, y_s, z_s)$ denoting a point over the source surface and $\mathbf{x} = (x, y, z)$ denoting the location of an observer. For simplicity, let the source be located at the plane $z_s = 0$, and let the origin of the coordinate system be located at the source centre; see Figure 2 for a representation of the problem.

Let r denote the distance between the source point $\mathbf{x}_s$ and the observer point $\mathbf{x}$; in the geometrical far-field, we can approximate the distance r as

$$r = \|\mathbf{x} - \mathbf{x}_s\| \approx \|\mathbf{x}\| - \frac{\mathbf{x} \cdot \mathbf{x}_s}{\|\mathbf{x}\|} \tag{1}$$

$$= \|\mathbf{x}\| - \|\mathbf{x}_s\| \cos(\theta). \tag{2}$$
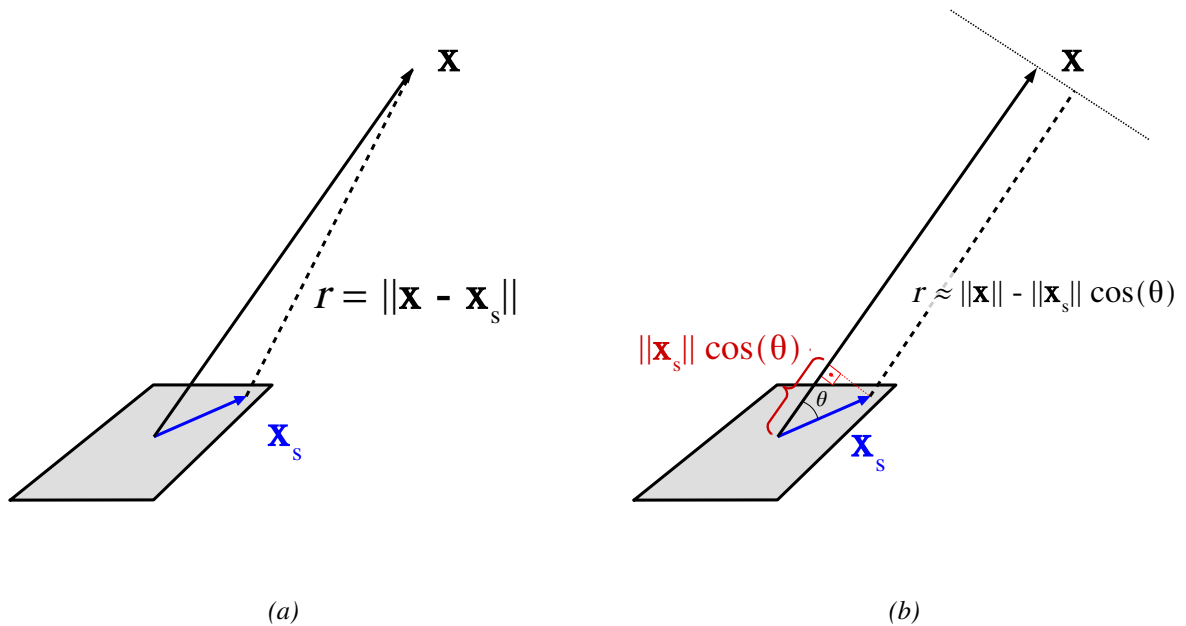

(a)   *(b)*

Figure 2: Geometrical arrangement for integrating extended sources: (a) considering the actual distance $r = \|\mathbf{x} - \mathbf{x}_s\|$ between observer and source; (b) considering the approximated distance $r \approx \|\mathbf{x}\| - \|\mathbf{x}_s\| \cos(\theta)$ using the Fraunhofer far-field approximation.

Equation 1 can be defined as the *Fraunhofer approximation*. The Authors have explored some concepts related to this approximation in a previous work [3], where it was derived by performing a Taylor series expansion of the source-observer propagation distance r and retaining the first-order terms only. It was also shown that for a fixed observer distance R, this approximation is valid for frequencies $f < f_{max}$, where

$$f_{max} = \frac{Rc_0}{\alpha D^2},\qquad(3)$$

where D is the source largest dimension, and α is a constant approximately equal to 2. At frequencies higher than f_{max}, the distance error becomes comparable to a maximum acceptable error and the approximation is not valid; the observer is then said to be in the *geometrical near-field* of the source.

3 THE SPATIAL FOURIER TRANSFORM

The Spatial Fourier Transform is a widely used technique for studying wave phenomena; it allows a scalar field in space to be decomposed into complex exponentials (i.e. plane waves) defined over a normally infinite two- or three-dimensional wavenumber space; this transform space includes waves with all possible wavelengths and directions of propagation within the original space.

Descriptions of this method for modelling acoustic wave propagation in a steady medium are available in many textbooks [7, 8, 17]. Recent examples of wavenumber analysis in aeroacoustics include wavenumber-space coherent deconvolution of the acoustic field recorded by a microphone array [1, 2]; wavenumber-domain analysis of pressure fluctuations beneath a compressible turbulent boundary layer in a flat plate[6]; and separation of acoustic components from convective components in acoustic array measurements by using beamforming[10, 13].

The Spatiotemporal Fourier Transform of a spatial variable $q(\mathbf{x},t)$ defined over the space $\mathbf{x} = (x,y,z)$ can be written as [11]

$$Q(k_x,k_y,k_z,\omega) = \iiiint_{-\infty}^{+\infty} q(x,y,z,t)e^{j\left(k_x x + k_y y + k_z z - \omega t\right)}\,\mathrm{d}t\,\mathrm{d}x\,\mathrm{d}y\,\mathrm{d}z.\qquad(4)$$

For a single-frequency variable that exists solely at the plane $z = 0$, the above equation simplifies to

$$Q(k_x,k_y,\omega) = \iint_{-\infty}^{+\infty} q(x,y,\omega)e^{jk_x x}e^{jk_y y}\,\mathrm{d}x\,\mathrm{d}y.\qquad(5)$$

Similarly, the Inverse Spatial Fourier Transform takes the form

$$q(x,y,\omega) = \frac{1}{(2\pi)^2}\iint_{-\infty}^{+\infty} Q(k_x,k_y,\omega)e^{-jk_x x}e^{-jk_y y}\,\mathrm{d}k_x\,\mathrm{d}k_y.\qquad(6)$$

4 SOUND RADIATION IN A MOVING MEDIUM

We now describe the relationship between the source strength distribution wavenumber spectrum and the acoustic far-field in a convected medium with mean flow of Mach number

$M_x = U_x/c_0$. All analyses done here are narrow-band and computed at a frequency ω, and the implicit time dependence is $e^{+j\omega t}$. Similar relationships can be obtained for steady medium conditions by assuming $M_x = 0$.

4.1 Acoustic Field Generated by a Continuous Source in Flow

The acoustic transfer function between a monopole source located at $\mathbf{x}_s$ and an observer located at $\mathbf{x}$ in a uniform flow and free-field conditions is defined by the convected Green's function

$$G_U(\mathbf{x}|\mathbf{x}_s, \omega) = \frac{e^{-jk_0\bar{r}}}{4\pi\beta^2\bar{r}}e^{jk_0M_x(\bar{\bar{x}}-\bar{\bar{x}}_s)}, \tag{7}$$

where the overline represents flow-transformed variables [4]:

$$\bar{\mathbf{x}} = (\bar{\bar{x}}, \bar{y}, \bar{z}) = \left(\frac{x}{\beta^2}, \frac{y}{\beta}, \frac{z}{\beta}\right), \quad \bar{r} = \|\bar{\mathbf{x}} - \bar{\mathbf{x}}_s\|, \quad \beta = \sqrt{1-M_x^2}. \tag{8}$$

We define a microphone array consisting of M observers at positions $\mathbf{x}_m$, all at a radius R from the source centre. A continuous monopole source distribution of strength $q(\mathbf{x}_s, \omega)$ and located over the plane $z_s = 0$ will generate an acoustic field at the m-th microphone location of the form

$$p(\mathbf{x}_m, \omega) = \int_{y_s}\int_{x_s} q(\mathbf{x}_s, \omega)G_U(\mathbf{x}_m|\mathbf{x}_s, \omega) \; \mathrm{d}x_s \, \mathrm{d}y_s. \tag{9}$$

Equation 9 fully describes the acoustic field produced by the source distribution $q(\mathbf{x}_s, \omega)$ at any observer position, but it has no analytical closed form. By assuming geometrical far-field conditions, we can use Eq. 1 in flow-transformed coordinates to approximate $\bar{r}$ in the convected Green's function and obtain a far-field-approximated Green's function of the form

$$G_{FF}(\mathbf{x}|\mathbf{x}_s, \omega) = e^{-jk_0\|\bar{\mathbf{x}}\|}e^{jk_0\frac{\bar{\mathbf{x}}\cdot\bar{\mathbf{x}}_s}{\|\bar{\mathbf{x}}\|}}\frac{1}{4\pi\sigma_{\mathbf{x}}}e^{jk_0M_x(\bar{\bar{x}}-\bar{\bar{x}}_s)} \tag{10}$$

$$= \frac{1}{4\pi\sigma_{\mathbf{x}}}e^{-j\hat{\mathbf{k}}\cdot(\mathbf{x}-\mathbf{x}_s)}, \tag{11}$$

where σ_m is the flow-corrected distance of the m-th observer to the source centre

$$\sigma_m = \sqrt{x_m^2 + \beta^2\left(y_m^2 + z_m^2\right)} = \beta^2\|\bar{\mathbf{x}}_m\|, \tag{12}$$

and $\hat{\mathbf{k}}_m$ is a wavenumber vector dependent on the m-th observer position of the form

$$\hat{\mathbf{k}}_m = \left(\hat{k}_{x,m}, \, \hat{k}_{y,m}, \, \hat{k}_{z,m}\right) \tag{13}$$

$$= \left(k_0\left(\frac{x_m - M_x\sigma_m}{\beta^2\sigma_m}\right), k_0\frac{y_m}{\sigma_m}, k_0\frac{z_m}{\sigma_m}\right). \tag{14}$$

Note that while the convected Green's function in Eq. 9 must be evaluated over flow-transformed spatial coordinates, its far-field approximation (Eq. 11) is a function of non-

transformed spatial coordinates; effectively, the far-field approximation allows us to express the convection effects in the wavenumber domain instead of the spatial domain.

We can then introduce Eq. 11 into Eq. 9 and rewrite it as

$$p(\mathbf{x}_m, \omega) \approx \frac{e^{-j\hat{\mathbf{k}}_m \cdot \mathbf{x}_m}}{4\pi\sigma_m} \int_{y_s} \int_{x_s} q(\mathbf{x}_s, \omega) e^{j\hat{\mathbf{k}}_m \cdot \mathbf{x}_s} \, \mathrm{d}x_s \, \mathrm{d}y_s. \tag{15}$$

Note that the double integral term in Eq. 15 is identical to a two-dimensional Spatial Fourier Transform of the source strength distribution evaluated at the wavenumber $\hat{\mathbf{k}}_m = (\hat{k}_{x,m}, \hat{k}_{y,m})$. We can then write

$$p(\mathbf{x}_m, \omega) \approx \frac{e^{-j\hat{\mathbf{k}}_m \cdot \mathbf{x}_m}}{4\pi\sigma_m} Q\left(\hat{k}_{x,m}, \hat{k}_{y,m}, \omega\right). \tag{16}$$

We propose the following interpretation of Eq. 16: the acoustic field seen by the observer at $\mathbf{x}_m$ is approximated by a plane wave of the form $e^{-j\hat{\mathbf{k}} \cdot \mathbf{x}}$, with complex amplitude given by $Q(\hat{k}_{x,m}, \hat{k}_{y,m})/4\pi\sigma_m$

By tracing the relationship between all possible observer locations over a hemisphere surrounding the acoustic source and their corresponding wavenumbers, we obtain the "acoustic domain" [10] of the wavenumber spectrum as all wavenumbers (k_x, k_y) contained inside the curve

$$\frac{(k_x + k_{x1})^2}{r_1^2} + \frac{k_y^2}{r_2^2} = 1, \tag{17}$$

where

$$k_{x1} = \frac{k_0 M_x}{\beta^2}, \quad k_{r1} = \frac{k_0}{\beta^2}, \quad k_{r2} = \frac{k_0}{\beta}. \tag{18}$$

Equation 17 represents an ellipse in the (k_x, k_y) plane, centred at $(-k_{x1}, 0)$ and with a semimajor axis k_{r1} and a semiminor axis k_{r2} [14], as shown in Figure 3; we refer to it as the "*radiation ellipse*". Wavenumber components located inside the ellipse correspond to waves reaching an observer in the far-field, while wavenumbers outside the ellipse correspond to evanescent waves and do not reach the far-field. In the absence of mean flow, the radiation ellipse reduces to a "*radiation circle*" of radius k_0, also shown in Figure 3.

4.2 Inverse Equation for Far-Field Source Estimation

We can now extend this methodology and write the inverse problem - estimating the source distribution from the far-field pressure measurements - as an Inverse Fourier Transform. Let us invert Eq. 16 and obtain an estimate of the source wavenumber spectrum from the acoustic far-field observations:

$$Q\left(\hat{k}_{x,m}, \hat{k}_{y,m}, \omega\right) \approx \left(\frac{e^{-j\hat{\mathbf{k}}_m \cdot \mathbf{x}_m}}{4\pi\sigma_m}\right)^{-1} p(\mathbf{x}_m, \omega). \tag{19}$$
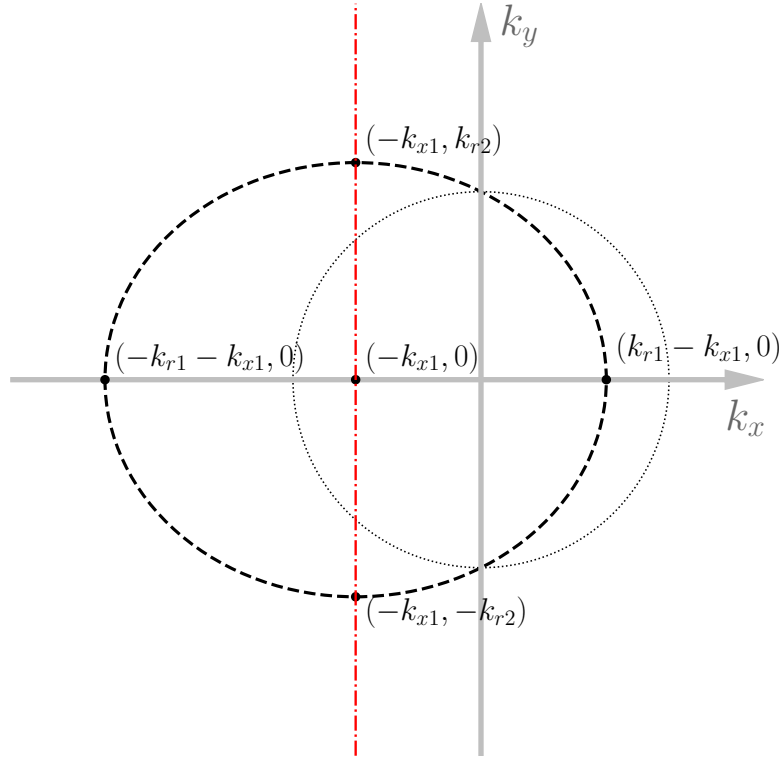
Figure 3: Radiation ellipse and radiation circle.

The observed far-field acoustic pressure provides an estimate to the source wavenumber spectrum at a particular wavenumber sample inside the radiation ellipse. Hence, if we can observe the acoustic far field over the entire hemisphere surrounding the source, it is possible to estimate the source spatial distribution via an Inverse Spatial Fourier Transform evaluated over the radiation ellipse:

$$q(x_s, y_s, \omega) \approx \frac{1}{(2\pi)^2} \int_{k_x} \int_{k_y} Q(k_x, k_y, \omega) e^{-j\mathbf{k} \cdot \mathbf{x}_s} \, dk_x \, dk_y, \quad (k_x, k_y) \in \text{Rad. Ellipse.} \qquad (20)$$

In practice, however, the acoustic field is sampled by the microphone array; the above integration in wavenumber domain then becomes a sum over the samples given by the M microphones:

$$q(x_s, y_s, \omega) \approx \frac{1}{(2\pi)^2} \sum_{m=0}^{M-1} Q(\hat{k}_{x,m}, \hat{k}_{y,m}, \omega) e^{-j\hat{\mathbf{k}}_m \cdot \mathbf{x}_s} \Delta S_m, \qquad (21)$$

where ΔS_m is an equivalent area in the wavenumber domain corresponding to the m-th microphone observation. These areas can be estimated using a modified Voronoi diagram of the array sampling in the wavenumber domain. Figure 4 shows this diagram for the array used in the first simulation example: red dots indicate the microphone samples, the dashed-dotted black line is the radiation ellipse, and the blue pentagons are the vertices of the Voronoi diagram that
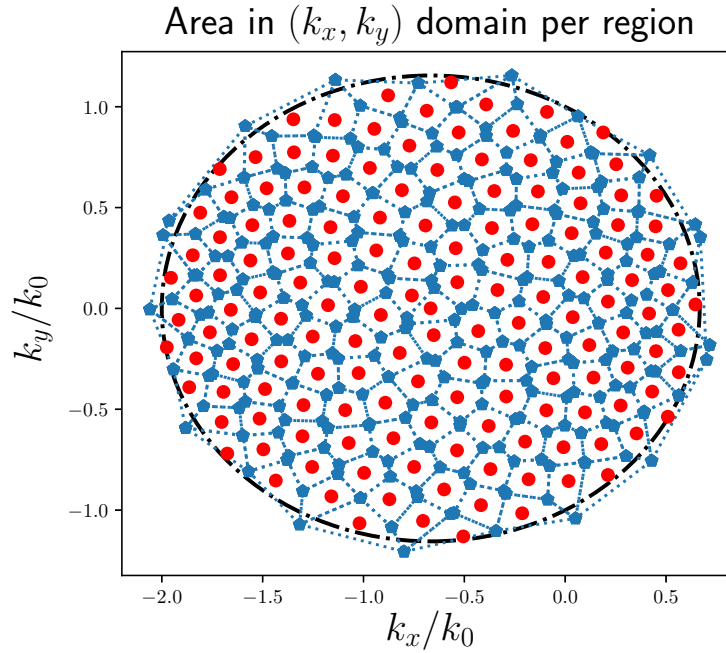
Figure 4: Example of estimation of equivalent area in wavenumber space using modified Voronoi diagram; see text for detailed description.

fall within or nearby the radiation domain.

5 MATRIX FORMULATION AND COMPARISON WITH CLASSICAL BEAMFORMING

We will now describe the same method in matrix form, and show how it compares to classical frequency-domain beamforming.

5.1 Matrix Formulation - Direct Problem

A single-frequency forward-propagation model can be described as follows: a vector $\mathbf{p}_{M \times 1}$ of acoustic pressure observations is related to a vector $\mathbf{q}_{N \times 1}$ of discretised source strengths via a matrix $\mathbf{G}_{M \times N}$ of transfer functions:

$$\mathbf{p} = \mathbf{G}\mathbf{q} \tag{22}$$

$$= \begin{bmatrix} | & | & & | \\ \mathbf{g}_0 & \mathbf{g}_1 & \cdots & \mathbf{g}_{N-1} \\ | & | & & | \end{bmatrix} \mathbf{q}. \tag{23}$$

Each vector $\mathbf{g}_n$ contains the transfer functions from the *n*-th source to all *M* observers and describes the type of acoustic propagation from source to receiver; for example, convected

point monopole (Eq. 7).

By populating the transfer function matrix **G** with the far-field-approximated point monopole transfer function (Eq. 11) we can write the direct problem in the far-field as

$$\mathbf{p} \approx \mathbf{G}^{FF}\mathbf{q} \tag{24}$$

$$= \begin{bmatrix} | & | & & | \\ \mathbf{g}_1^{FF} & \mathbf{g}_2^{FF} & \cdots & \mathbf{g}_N^{FF} \\ | & | & & | \end{bmatrix} \mathbf{q} \tag{25}$$

$$= \begin{bmatrix} \dfrac{e^{-j\hat{\mathbf{k}}_0 \cdot \mathbf{x}_0}}{4\pi\sigma_0}e^{j\hat{\mathbf{k}}_0 \cdot \mathbf{x}_{s0}} & \cdots & \dfrac{e^{-j\hat{\mathbf{k}}_0 \cdot \mathbf{x}_0}}{4\pi\sigma_0}e^{j\hat{\mathbf{k}}_0 \cdot \mathbf{x}_{s(N-1)}} \\ \vdots & \ddots & \vdots \\ \dfrac{e^{-j\hat{\mathbf{k}}_{M-1} \cdot \mathbf{x}_{M-1}}}{4\pi\sigma_{M-1}}e^{j\hat{\mathbf{k}}_{M-1} \cdot \mathbf{x}_{s0}} & \cdots & \dfrac{e^{-j\hat{\mathbf{k}}_{M-1} \cdot \mathbf{x}_{M-1}}}{4\pi\sigma_{M-1}}e^{j\hat{\mathbf{k}}_{M-1} \cdot \mathbf{x}_{s(N-1)}} \end{bmatrix} \mathbf{q} \tag{26}$$

$$= \begin{bmatrix} \dfrac{e^{-j\hat{\mathbf{k}}_0 \cdot \mathbf{x}_0}}{4\pi\sigma_0} & \cdots & 0 \\ \vdots & \ddots & \vdots \\ 0 & \cdots & \dfrac{e^{-j\hat{\mathbf{k}}_{M-1} \cdot \mathbf{x}_{M-1}}}{4\pi\sigma_{M-1}} \end{bmatrix} \begin{bmatrix} e^{j\hat{\mathbf{k}}_0 \cdot \mathbf{x}_{s0}} & \cdots & e^{j\hat{\mathbf{k}}_0 \cdot \mathbf{x}_{s(N-1)}} \\ \vdots & \ddots & \vdots \\ e^{j\hat{\mathbf{k}}_{M-1} \cdot \mathbf{x}_{s0}} & \cdots & e^{j\hat{\mathbf{k}}_{M-1} \cdot \mathbf{x}_{s(N-1)}} \end{bmatrix} \mathbf{q} \tag{27}$$

$$= \mathbf{REq}. \tag{28}$$

Thus, the direct problem in the far-field can be written as the product of a diagonal matrix $\mathbf{R}_{M \times M}$ containing the phase shifts and attenuation related to the observer location, and a Fourier Transform-like matrix $\mathbf{E}_{M \times N}$ mapping the source strength at $\mathbf{x}_{sn}$ to a observer-dependent wavenumber $\mathbf{k}_m$.

The direct problem can then be expressed as

$$\mathbf{p} \approx \mathbf{G}^{FF}\mathbf{q} \tag{29}$$

$$= \mathbf{REq} \tag{30}$$

$$= \mathbf{Rq}_k, \tag{31}$$

where $\mathbf{q}_k = [Q[0], \ldots, Q[M-1]]^T$ is a vector of source strength Spatial Fourier Transform samples evaluated at the M discrete wavenumbers $\hat{\mathbf{k}}[m]$.

If we instead desire to obtain the cross-spectrum $\mathbf{C}_{pp}$ of the acoustic pressures, it can be easily formulated from the cross-spectrum $\mathbf{C}_{kk}$ of the source wavenumber spectrum or of the cross-spectrum $\mathbf{C}_{qq}$ of the spatial source distribution:

$$\mathbf{C}_{pp} = \mathrm{E}\left\{\mathbf{pp}^H\right\} \tag{32}$$

$$= \mathbf{RE}\,\mathrm{E}\left\{\mathbf{qq}^H\right\}\,\mathbf{E}^H\mathbf{R}^H \tag{33}$$

$$= \mathbf{REC}_{qq}\mathbf{E}^H\mathbf{R}^H \tag{34}$$

$$= \mathbf{RC}_{kk}\mathbf{R}^H. \tag{35}$$

5.2 Matrix Formulation - Inverse Problem

We would like to invert the above equation and obtain an estimate $\tilde{\mathbf{q}}$ of the source strength vector $\mathbf{q}$. A first step is to obtain an estimate $\tilde{\mathbf{q}}_k$ of the source strength Spatial Fourier Transform from the vector of microphone complex pressures:

$$\tilde{\mathbf{q}}_k = \mathbf{R}^\dagger\mathbf{p}, \tag{36}$$

where $\mathbf{R}^\dagger$ is the inverse of $\mathbf{R}$:

$$\mathbf{R}^\dagger_{M\times M} = \mathbf{R}^{-1} \tag{37}$$

$$= \begin{bmatrix} \left(e^{j\hat{\mathbf{k}}_0\cdot\mathbf{x}_0}\right)4\pi\sigma_0 & 0 & \dots & 0 \\ 0 & \left(e^{j\hat{\mathbf{k}}_1\cdot\mathbf{x}_1}\right)4\pi\sigma_1 & \dots & 0 \\ \vdots & \vdots & \ddots & \vdots \\ 0 & 0 & \dots & \left(e^{j\hat{\mathbf{k}}_{M-1}\cdot\mathbf{x}_{M-1}}\right)4\pi\sigma_{M-1} \end{bmatrix}. \tag{38}$$

Since the matrix $\mathbf{R}$ only contains the attenuations and phase shifts related to the microphone positions, its inverse is not ill-conditioned and can be inverted numerically. Finally, from $\tilde{\mathbf{q}}_k$, we can compute the source distribution estimate $\tilde{\mathbf{q}}$ by performing an Inverse Spatial Fourier Transform - i.e. left-multiplying by $\mathbf{E}^H$:

$$\tilde{\mathbf{q}} = \mathbf{E}^H\tilde{\mathbf{q}}_k \tag{39}$$

$$= \mathbf{E}^H\mathbf{R}^\dagger\mathbf{p}. \tag{40}$$

Therefore, the source estimation procedure consists of inverting a well-conditioned diagonal matrix and taking the complex-conjugate of a matrix of phase shifts; all these steps are easily calculated.

Once again, if we desire to obtain an estimate $\tilde{\mathbf{C}}_{qq}$ of the source strength cross-spectrum, it can be simply formulated as

$$\tilde{\mathbf{C}}_{qq} = \mathrm{E}\left\{\tilde{\mathbf{q}}\tilde{\mathbf{q}}^H\right\} \tag{41}$$

$$= \mathbf{E}^H\mathbf{R}^\dagger\,\mathrm{E}\left\{\mathbf{pp}^H\right\}\,\mathbf{R}^{\dagger H}\mathbf{E} \tag{42}$$

$$= \mathbf{E}^H\mathbf{R}^\dagger\mathbf{C}_{pp}\mathbf{R}^{\dagger H}\mathbf{E}. \tag{43}$$

5.3 Comparison with Classical Beamforming

A beamformer can be described as a weighted linear combination of the array sensor signals that estimates the source strength at one scanning location; let $\mathbf{w}_n$ denote the vector of M complex weights that allows the estimation of the n-th source strength q_n:

$$\tilde{q}_n = \mathbf{w}_n^H \mathbf{p}. \tag{44}$$

We will call the vector $\mathbf{w}_n$ the *steering vector*. Many formulations for steering vectors are possible, and are generally calculated from the assumed transfer function matrix entries. We propose a vector-wise inversion of the entries of the transfer function $\mathbf{G}$ as our steering vector:

$$\mathbf{w}_n = \frac{\mathbf{g}_n}{\|\mathbf{g}_n\|^2}. \tag{45}$$

Equation 45 can be obtained by minimizing the difference $\|\mathbf{p} - q_n\mathbf{g}_n\|^2$ (see Sijtsma[15]), and correctly recovers the source strength for the case of a single point source located at the scanning position.

The vector of estimated source strengths is given by

$$\tilde{\mathbf{q}} = \mathbf{W}^H \mathbf{p} \tag{46}$$

$$= \begin{bmatrix} - & \mathbf{w}_1^H & - \\ - & \mathbf{w}_2^H & - \\ & \vdots & \\ - & \mathbf{w}_N^H & - \end{bmatrix} \mathbf{p} \tag{47}$$

$$\tag{48}$$

If we choose to populate our transfer function matrix with far-field Green's functions, our steering vector can be written as

$$w_{m,n}^{FF} = \left(e^{-j\hat{\mathbf{k}}_m \cdot \mathbf{x}_n} 4\pi\sigma_m \right) e^{j\hat{\mathbf{k}}_m \cdot \mathbf{x}_{sn}}. \tag{49}$$

The Inverse Problem can be written as

$$\tilde{\mathbf{q}} = \mathbf{W}^H \mathbf{p} \tag{50}$$

$$= \begin{bmatrix} - & \mathbf{w}_1^H & - \\ - & \mathbf{w}_2^H & - \\ & \vdots & \\ - & \mathbf{w}_N^H & - \end{bmatrix} \mathbf{p} \tag{51}$$

$$= \begin{bmatrix} \left(e^{j\hat{\mathbf{k}}_0 \cdot \mathbf{x}_0} 4\pi\sigma_0\right) e^{-j\hat{\mathbf{k}}_0 \cdot \mathbf{x}_{s0}} & \cdots & \left(e^{j\hat{\mathbf{k}}_{M-1} \cdot \mathbf{x}_{M-1}} 4\pi\sigma_{M-1}\right) e^{-j\hat{\mathbf{k}}_{M-1} \cdot \mathbf{x}_{s0}} \\ \vdots & \ddots & \vdots \\ \left(e^{j\hat{\mathbf{k}}_0 \cdot \mathbf{x}_0} 4\pi\sigma_0\right) e^{-j\hat{\mathbf{k}}_0 \cdot \mathbf{x}_{s(N-1)}} & \cdots & \left(e^{j\hat{\mathbf{k}}_{M-1} \cdot \mathbf{x}_{M-1}} 4\pi\sigma_{M-1}\right) e^{-j\hat{\mathbf{k}}_{M-1} \cdot \mathbf{x}_{s(N-1)}} \end{bmatrix} \mathbf{p} \tag{52}$$

$$= \begin{bmatrix} e^{-j\hat{\mathbf{k}}_0 \cdot \mathbf{x}_{s0}} & \cdots & e^{-j\hat{\mathbf{k}}_{M-1} \cdot \mathbf{x}_{s0}} \\ \vdots & \ddots & \vdots \\ e^{-j\hat{\mathbf{k}}_0 \cdot \mathbf{x}_{s(N-1)}} & \cdots & e^{-j\hat{\mathbf{k}}_{M-1} \cdot \mathbf{x}_{s(N-1)}} \end{bmatrix} \begin{bmatrix} \left(e^{j\hat{\mathbf{k}}_0 \cdot \mathbf{x}_0} 4\pi\sigma_0\right) & \cdots & 0 \\ \vdots & \ddots & \vdots \\ 0 & \cdots & \left(e^{j\hat{\mathbf{k}}_{M-1} \cdot \mathbf{x}_{M-1}} 4\pi\sigma_{M-1}\right) \end{bmatrix} \mathbf{p} \tag{53}$$

$$= \mathbf{E}^H \mathbf{R}^\dagger \mathbf{p}. \tag{54}$$

Given that Equation 54 is identical to Eq. 40, the beamforming formulation as computed from a far-field approximated Green's function is identical to the proposed Fourier-based formulation. Of course, it follows from the above that the expressions for beamforming with the cross-spectral matrix will also be identical to the proposed formulations.

6 SIMULATIONS

We now present some simulation results by implementing the proposed method in Python programming language. All arrays presented here are designed as a "sunflower" spiral pattern [16] in the 2D (x, y) plane, and are then extrapolated to the hemisphere above the source; this allows for an arbitrary number of microphones to be positioned in the hemisphere in an approximately uniform distribution in wavenumber domain. The array is positioned far enough from the source so that Eq. 3 is satisfied.

The simulated source is rectangular, with a deterministic, narrowband source strength distribution given by a single complex exponential; the source dimensions are $(D_x, D_y) = (\lambda_0, 1.5\lambda_0)$, and the mean flow Mach number is $M_x = 0.5$. The acoustic field at the microphones is obtained via a numerical evaluation of Eq. 9 (using the exact Green's function - Eq. 7), and the inversion steps follow the method described above using the far-field-approximated Green's function (Eq. 11).

The estimated wavenumber spectrum is evaluated at the $\hat{\mathbf{k}}_m$ points corresponding to each microphone using Eq. 19. In the next examples, regions between the wavenumber samples have been interpolated and are shown for visualisation purposes only; all results are obtained from the discrete wavenumber spectrum only. We also define a relative source estimation error of the form

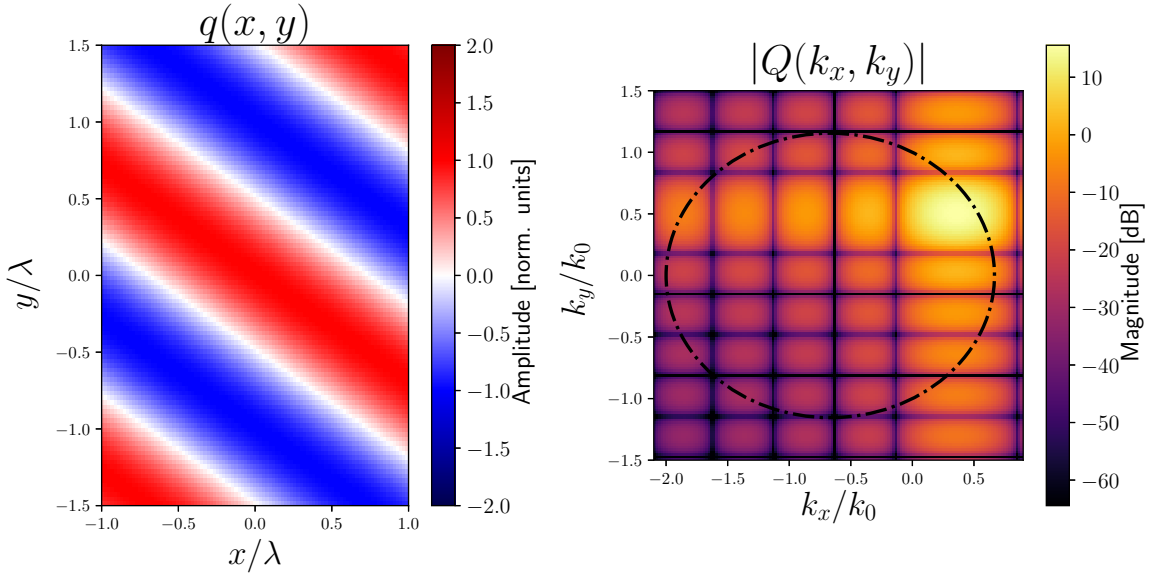$$q_{error}(x, y) = q(x, y) - \tilde{q}(x, y), \tag{55}$$

Figure 5: Source strength distribution (left) and wavenumber spectra (right), with radiation ellipse indicated in wavenumber domain; the Mach number is $M_x = 0.5$.

and we plot this source error as a metric to evaluate the source estimation process.

6.1 Simulated Case 1: Planar Radiator, Hemispherical Array

Case 1 is shown in Figure 6 and consists of a hemispherical array covering the entire angular above the source; there are 150 microphones positioned in the source far-field, at equal distance from source centre. Clearly, this is a highly impractical array due to large number of microphones and wide spatial coverage; however, the source wavenumber spectrum is well sampled inside the radiating ellipse, including the source main lobe.

The source spatial distribution is recovered moderately well; some inaccuracies are visible, although overall levels and spatial characteristics are correctly recovered. Inaccuracies might be due to the lack of evanescent components, which can't reach the far-field and are responsible for the fine details of the source spatial structure; the estimation error is concentrated along the edges of the source, where there are sharp transitions corresponding to high spatial frequency phenomena.

6.2 Simulated Case 2: Planar Radiator, Spherical Cap Array

Case 2 is shown in Figure 7 and consists of a spherical cap array, covering a section of the hemisphere immediately above the source; there are 75 microphones positioned in the source far-field, at equal distance from the source centre. This array is closer to what actual laboratory experimental conditions would be than the previous array; however, the source wavenumber spectrum is not well sampled inside radiating ellipse, and does not include the main lobe.

The source spatial distribution is recovered poorly; overall levels and spatial characteristics are entirely misrepresented, and the estimation error is high over the entire source surface. In-
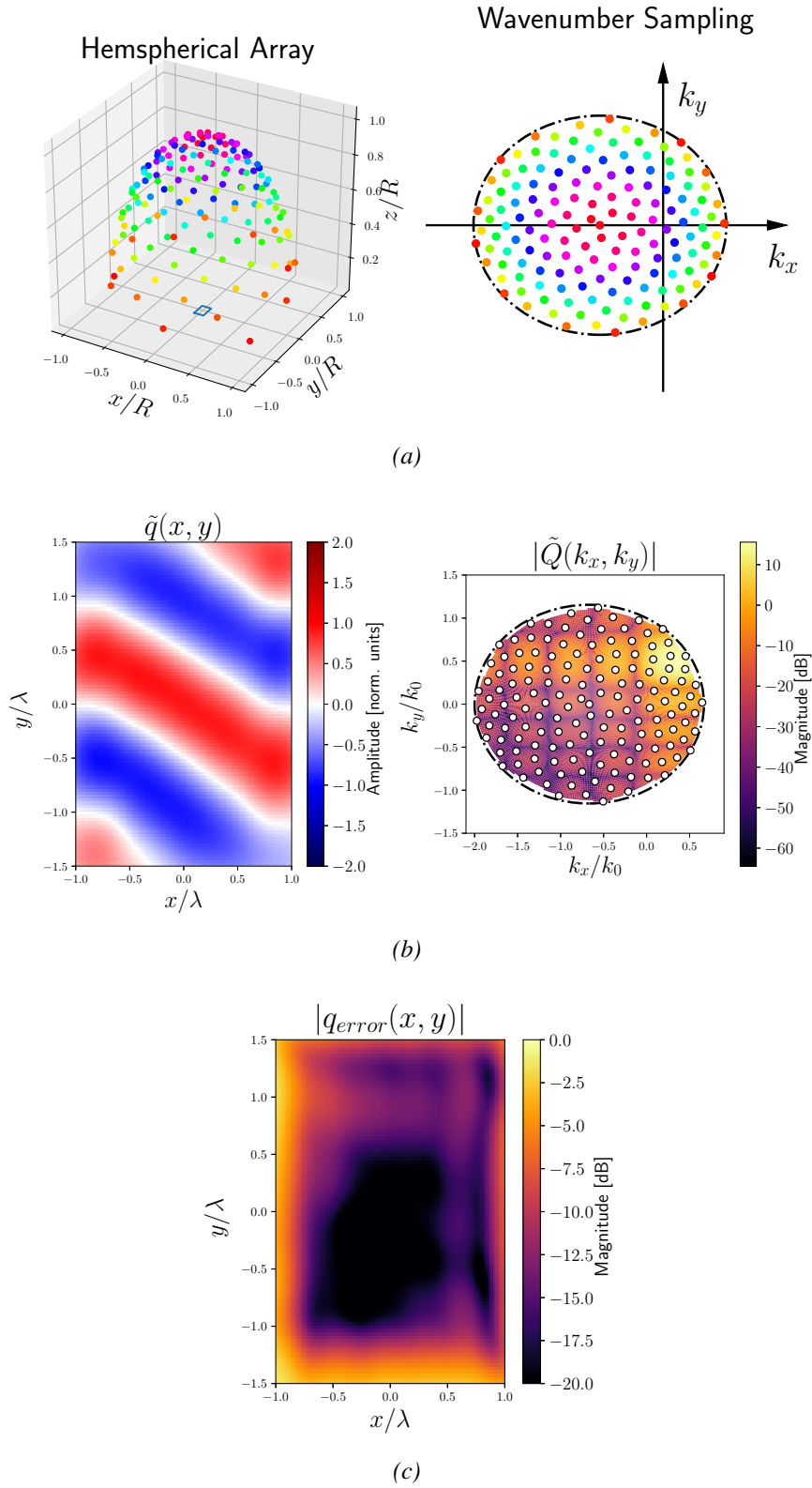
(a)

(b)

(c)

Figure 6: Case 1: Hemispherical array covering the entire angular space: (a) Microphone positions in spatial domain and wavenumber domain; (b) Estimated source spatial distribution and wavenumber spectrum; (c) Source estimation error in spatial domain.

14

accuracies might be due the lack of strongly energetic components, since the "visibility region" of this array consists only of sidelobes and contains many nulls. It is worth noting that the main spatial component is absent from the measurements, and hence made "invisible".

6.3 Simulated Case 3: Planar Radiator, Modified Cap Array

Case 3 is shown in Figure 8 and consists of a modified cap array, similar to Case 2, but covering a different section of the hemisphere - this time closer to the main radiation lobe. Once again, there are 75 microphones positioned in the source far-field and at equal distance from the source centre. This is an impractical array design due to non-uniform sampling of the angular domain and awkward microphone positioning. The source wavenumber spectrum is again not well sampled inside radiating ellipse, but for this case it does include a significant portion of the main radiation lobe.

The source spatial distribution is partially recovered, with overall levels and spatial characteristics are approximately represented, if perhaps not very accurately. Inaccuracies might be due the lack of the remaining wavenumber components, responsible for the finer details; while the estimation errors are higher than in the first case, these are again concentrated along the edges of the source, where high frequency phenomena are expected.

7 CONCLUSIONS

We have presented a method relating the Spatial Fourier Transform of a source distribution to its radiated acoustic far-field, and proposed an inversion method to obtain the source distribution from the far-field measurements. This framework is valid for acoustic propagation in both steady and convected media, and it arrives at some of the already-known limitations in array signal processing from a slightly different perspective.

The proposed wavenumber space sampling is directly dependent on the microphone array geometry, but through a non-uniform mapping into k-space; a uniform sampling in wavenumber domain requires an array with a dense arrangement of microphones immediately above the source, and a sparser arrangement towards the sides of the hemisphere. Of course, the reverse is also valid: a uniform arrangement of microphones in the angular domain will lead to a non-uniform arrangement in the wavenumber domain.

There is a direct association between the angular aperture of a given microphone array and which wavenumber components it can successfully recover - i.e. each array has an equivalent "*visibility region*" in the wavenumber domain. Different array apertures and positions will observe different portions of the wavenumber spectrum, changing which components can be estimated; this has a direct consequence on the source distribution estimation in the spatial domain, as demonstrated in the simulations.

Another consequence of performing measurements in the far-field is that evanescent wavenumber components - outside of the radiation ellipse - cannot be observed by definition. This imposes a spatial resolution limit on the source distribution estimation, since high spatial frequency phenomena (i.e. fine details) cannot be observed. It is expected that measurements performed in the near-field should be able to recover some evanescent components, although to what exact extent is still not known.
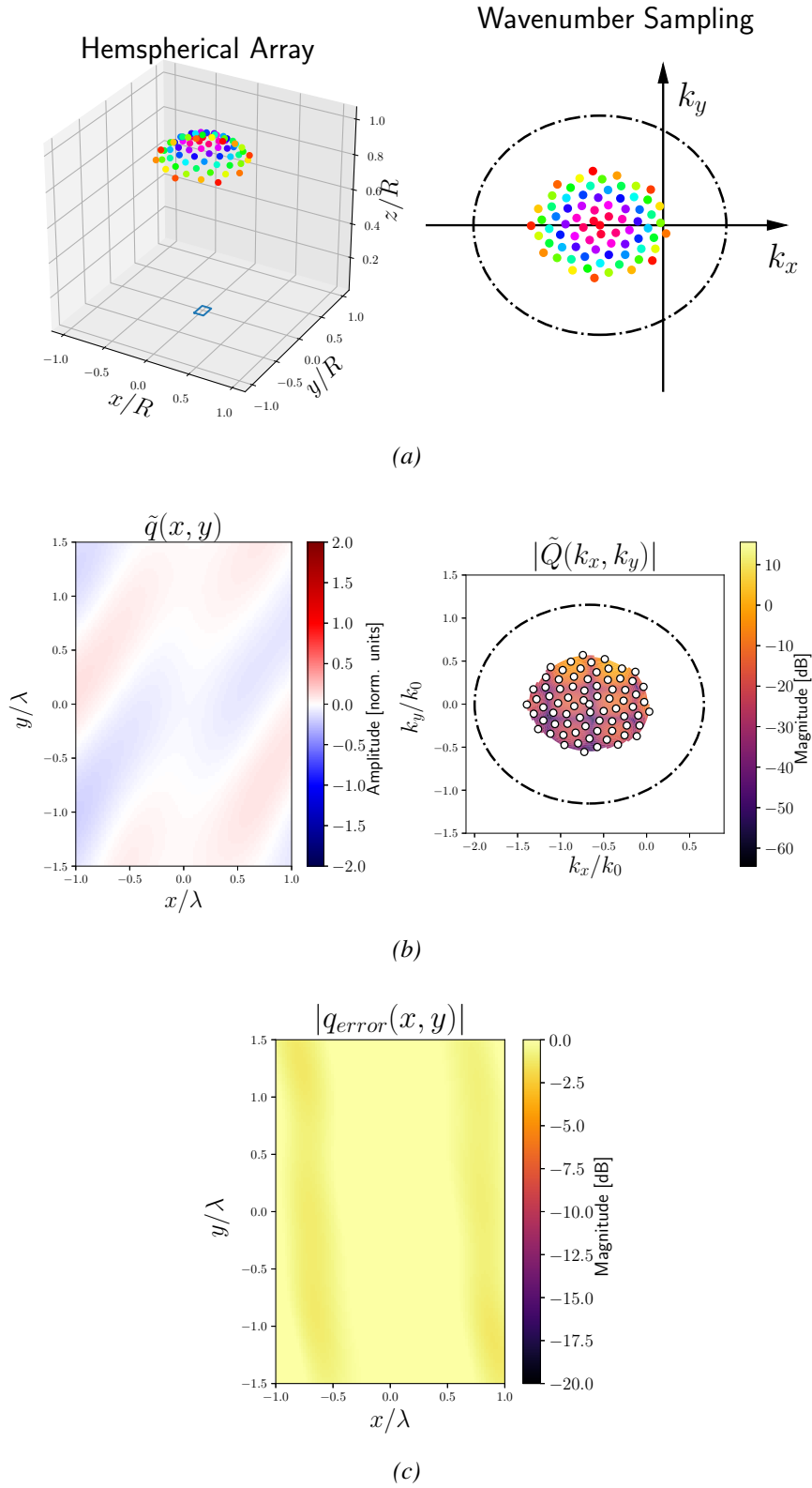
(a)

(b)

(c)

Figure 7: Case 2: Hemispherical cap array covering a portion of the angular space: (a) Microphone positions in spatial domain and wavenumber domain; (b) Estimated source spatial distribution and wavenumber spectrum; (c) Source estimation error in spatial domain.
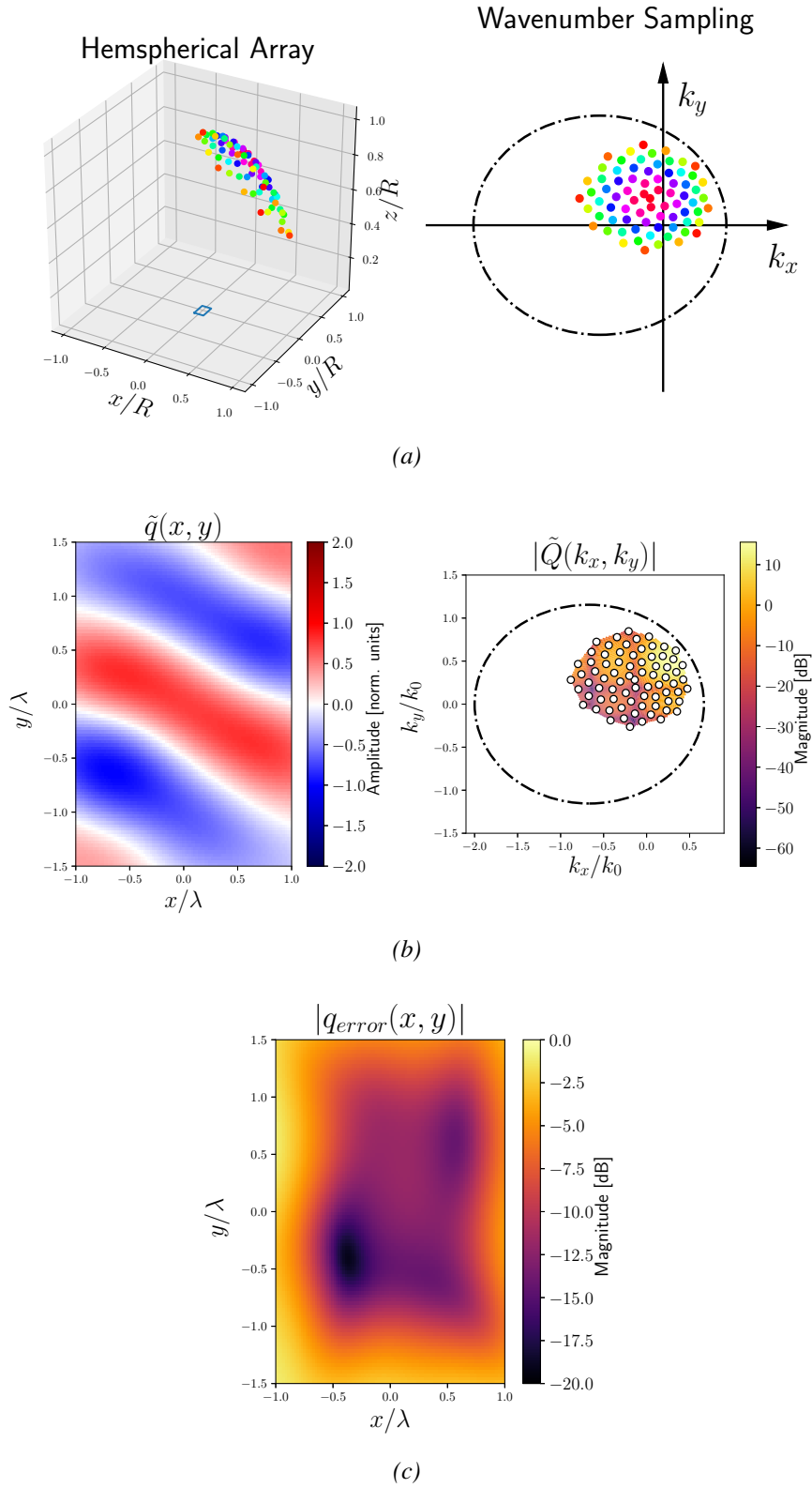
(a)

(b)

(c)

Figure 8: Case 3: Modified cap array covering a portion of the angular space: (a) Micro-phone positions in spatial domain and wavenumber domain; (b) Estimated source spatial distribution and wavenumber spectrum; (c) Source estimation error in spatial domain.

17

Finally, while the spatial resolution limit might be considered a disadvantage when attempting to recovering the exact source spatial distribution, we can also interpret the method as an estimation of the source radiating behaviour only; such "equivalent source" description should explain the source far-field behaviour and ignore components that do not affect the far-field.

Acknowledgments

References

[1] C. Bahr and L. Cattafesta. "Wavespace-based coherent deconvolution." In *18th AIAA/CEAS Aeroacoustics Conference*. 2012. AIAA Paper 2012-2227.

[2] C. Bahr and L. Cattafesta. "Wavenumber-frequency deconvolution of aeroacoustic microphone phased array data of arbitrary coherence." *Journal of Sound and Vibration*, Vol. 382, 13–42, 2016.

[3] F. Casagrande Hirono, P. Joseph, and F. Fazi. "Aerofoil source estimation from nearfield array measurements." In *23rd AIAA/CEAS Aeroacoustics Conference*. 2017. AIAA Paper 2017-4178.

[4] C. J. Chapman. "Similarity variables for sound radiation in a uniform flow." *Journal of Sound and Vibration*, Vol. 233, No. 1, 157–164, 2000.

[5] A. Dowling and J. Ffowcs Williams. *Sound and Sources of Sound*. Ellis Horwood, Chichester, UK, 1983.

[6] K. Ehrenfried and L. Koop. "Experimental study of pressure fluctuations beneath a compressible turbulent boundary layer." In *14th AIAA/CEAS Aeroacoustics Conference*. 2008. AIAA Paper 2008-2800.

[7] F. Fahy and P. Gardonio. *Sound and Structural Vibration*. Academic Press, Oxford, UK, 2007.

[8] S. Glegg and W. Devenport. *Aeroacoustics of Low Mach Number Flows*. Elsevier Academic Press, London, UK, 2017.

[9] J. Goodman. *Introduction to Fourier Optics*. Roberts & Company, Colorado, USA, 2005.

[10] S. Haxter and C. Spehr. "Infinite beamforming: Wavenumber decomposition of surface pressure fluctuations." In *5th Berlin Beamforming Conference*. 2014. BeBeC Paper BeBeC-2014-04.

[11] D. Johnson and D. Dudgeon. *Array Signal Processing*. Prentice-Hall, New Jersey, USA, 1993.

[12] L. Kinsler, A. Frey, A. Coppens, and J. Sanders. *Fundamentals of Acoustics*. John Wiley and Sons, London, UK, 2000.

[13] L. Koop and K. Ehrenfried. "Microphone-array processing for wind-tunnel measurements with strong background noise." In *14th AIAA/CEAS Aeroacoustics Conference*. 2008. AIAA Paper 2008-2907.

[14] H.-S. Kwon, Y. Niu, and Y.-J. Kim. "Planar nearfield acoustical holography in moving fluid medium at subsonic and uniform velocity." *Journal of the Acoustical Society of America*, Vol. 126, 1823–1832, 2010.

[15] P. Sijtsma. "Phased array beamforming applied to wind tunnel and fly-over tests." Technical Report NLR-TP-2010-549, National Aerospace Laboratory (NLR) - the Netherlands, 2010.

[16] H. Vogel. "A better way to construct the sunflower head." *Mathematical Biosciences*, Vol. 44, 179–189, 1979.

[17] E. Williams. *Fourier Acoustics: Sound Radiation and Nearfield Acoustical Holography*. Academic Press, London, UK, 1999.